Electrical Transport and Field-Effect Transistors Using Inkjet-Printed SWCNT Films Having Different Functional Side Groups

Eduardo Gracia-Espino,[†,‡] Giovanni Sala,[‡] Flavio Pino,[‡] Niina Halonen,[‡] Juho Luomahaara,[§] Jani Mäklin,[‡] Géza Tóth,[‡] Krisztián Kordás,[‡] Heli Jantunen,[‡] Mauricio Terrones,[⊥] Panu Helistö,[§] Heikki Seppä,[§] Pulickel M. Ajayan,[∥] and Robert Vajtai[∥,*]

[†]Advanced Materials Department, Instituto Potosino de Investigación Científica y Tecnológica, camino a la presa San José 2055, Col. Lomas 4. Sección, 78216 San Luis Potosí, México, [‡]Microelectronics and Materials Physics Laboratories, Department of Electrical and Information Engineering, University of Oulu, P.O. Box 4500, FIN-90014 University of Oulu, Finland, [§]Quantronics/Microtechnologies and Sensors, VTT Technical Research Centre of Finland, Espoo, P.O. Box 1000, TT3, 02044 VTT, Finland, [⊥]Departamento de Ciencia e Ingeniería de Materiales e Ingeniería Química, Escuela Politécnica Superior, Universidad Carlos III de Madrid, Avenida Universidad 30, 28911 Leganés, Madrid, Spain, and [∥]Department of Mechanical Engineering and Materials Science, Rice University, Houston, Texas 77005

ABSTRACT The electrical properties of random networks of single-wall carbon nanotubes (SWNTs) obtained by inkjet printing are studied. Water-based stable inks of functionalized SWNTs (carboxylic acid, amide, poly(ethylene glycol), and polyaminobenzene sulfonic acid) were prepared and applied to inkjet deposit microscopic patterns of nanotube films on lithographically defined silicon chips with a back-side gate arrangement. Source—drain transfer characteristics and gate-effect measurements confirm the important role of the chemical functional groups in the electrical behavior of carbon nanotube networks. Considerable nonlinear transport in conjunction with a high channel current on/off ratio of ~70 was observed with poly(ethylene glycol)-functionalized nanotubes. The positive temperature coefficient of channel resistance shows the nonmetallic behavior of the inkjet-printed films. Other inkjet-printed field-effect transistors using carboxyl-functionalized nanotubes as source, drain, and gate electrodes, poly(ethylene glycol)-functionalized nanotubes as the channel, and poly(ethylene glycol) as the gate dielectric were also tested and characterized.

Single-wall carbon nanotubes (SWCNTs) are appealing candidates for fabricating molecular electronics devices. Depending on their chirality, SWCNTs could exhibit either metallic (m-CNT) or semiconducting (s-CNT) behavior, both necessary building blocks for constructing electronic circuits.[1] Different techniques have been reported for the fabrication of devices based on individual SWCNTs, including field-effect transistors and logic circuits,[2] gas sensors,[3] and nano-sized rectifiers.[4] However, the assembly and connection of individual SWCNTs to contacts is challenging, and the absence of highly purified SWCNTs of specific chirality complicates the assembly of electronic devices based on individual SWCNTs.

Carbon nanotube films have been explored as an alternative solution for constructing electronics devices. The viability of using SWCNT networks as diodes and field-effect transistors (FETs)[5−8] and chemical sensors[9,10] has already been demonstrated. Additionally, because of their optical transparency and electrical conduction, SWCNT films have been suggested for conductive coatings as an alternative to transparent oxides.[11,12] Random arrays of SWCNTs are easily produced by their deposition onto an arbitrary substrate from a solution of suspended SWCNTs, using different techniques such as vacuum filtration, electrophoretic deposition, dip and spray coating,[13] as well as by inkjet printing.[14−16] If the density of SWCNTs in such an array is sufficiently high (*i.e.*, exceeds the percolation limit), the nanotubes will interconnect and form continuous electrical paths between the electrodes. Low density (but percolated) films of SWCNTs exhibit nonlinear current—voltage behavior and show gate-modulated transport in the channel due to the Schottky barriers forming at the interface of metallic and semiconducting nanotubes. Thick layers, in which the metallic nanotubes can form continuous electrical paths between probe electrodes, have linear transport properties without showing any gate control.[15−17]

Chemical surface modification of nanotubes by attaching functional groups has been utilized as an important step for pre-
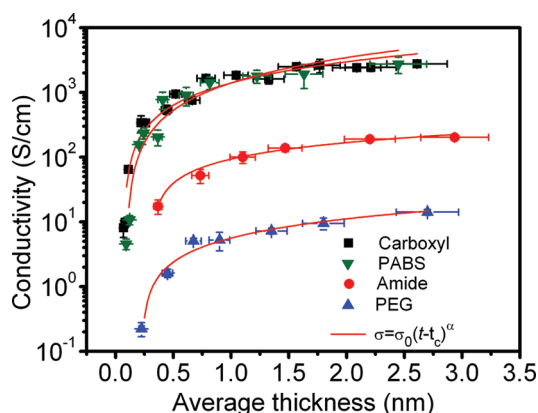
Figure 1. Electrical conductivity as a function of average film thickness of SWCNT networks made of four different types of functionalized nanotubes. Various thicknesses were obtained by subsequent printing over the same pattern. The electrical resistances of all networks were tested at −5 V drain−source bias. Depending on film thickness, the conductivity of the films can be varied within a window of ∼2 orders of magnitude.

paring suspensions and stable solutions. However, the original electrical properties of the nanotubes are not left intact, which is to be taken into account when designing a new device.[18] Side wall covalent functionalization and vacancy defects that change the sp^2 hybridization of carbon atoms in the tube wall could induce an impurity state in the gap region, thus leading to considerable change in electronic states as well as in the electrical properties of nanotubes. This appears to be independent from the functional groups (provided those are monovalent) as obtained by *ab initio* calculations.[19,20] By introducing different chemical groups to the nanotube wall, it is possible to change the interaction between nanotubes and the surrounding environment. This reactivity could enhance the sensitivity and selectivity of CNT-based gas sensor devices.[21,22]

In this work, we study the electrical properties of thin films of inkjet-deposited SWCNT networks with different types of functional groups: carboxylic acid (−COOH), amide (−CONH$_2$), poly(ethylene glycol) (PEG), and polyaminobenzene sulfonic acid (PABS). We then show different device operations caused by the chemical groups. In addition, we demonstrate the construction of entirely inkjet-printed field-effect transistors using well conducting thick layers of carboxyl-functionalized nanotubes as source, drain, and gate electrodes, semiconducting films of PEG-functionalized nanotubes as channel and PEG as the gate dielectric.

RESULTS AND DISCUSSION

A series of SWCNT films with different thickness were deposited on SiO$_2$ substrates to form random networks of partially bundled SWCNTs. The electrical conductivity (Figure 1) of the films was calculated from resistance measurements carried out at 5 V channel bias. By increasing the thickness of the nanotube networks,

TABLE 1. Calculated Percolation Threshold Thickness t_c (Average over the Printed Surface Area) and Critical Exponent α for the Deposited Nanotube Films

	carboxyl	amide	PEG	PABS
t_c (nm)	0.07 ± 0.01	0.31 ± 0.05	0.23 ± 0.38	0.09 ± 0.02
α	1.03 ± 0.11	0.65 ± 0.15	0.83 ± 0.54	1.22 ± 0.27

the conductivity of each film increases ∼2 orders of magnitude within a narrow thickness window of the experiments; however, above a certain critical thickness, further significant increment of conductivity cannot be reached. Despite the equivalent nanotube coverage, the conductivities are different for each type of film. Carboxylated and PABS-functionalized nanotubes exhibit always the lowest resistivity, followed by amide and PEG-functionalized films having corresponding sample thickness values.

The overall conductivity *versus* thickness behavior measured for each film is similar to those of percolating networks. Near the percolation threshold (p_c), the conductivity (σ) is expected to be related to the concentration of conducting paths (p) by the universal power law of the form $\sigma \propto (p - p_c)^{\alpha}$.[23,24] As the conducting paths are proportional to the film thickness, the conductivity law can be expressed as $\sigma \propto (t - t_c)^{\alpha}$ for $t \geq t_c$, where t and t_c are the thickness and the corresponding threshold value (critical thickness), and α is the critical exponent. For thicknesses lower than t_c, there is no connection between the contact electrodes. Over the threshold limit, in the SWCNT networks, the overall resistance is dominated by the tube−tube, tube−bundle, and bundle−bundle contacts as well as by the intrinsic conductivities of the nanotubes. By increasing the film thickness, the number of percolated paths increases, thus the resistance decreases as more and more parallel connections form. However, at high film thicknesses, addition of further nanotubes to the network cannot contribute much to the improvement of conductivity because the film becomes like an ideal bulk conductor (∼2 nm thickness for each sample).

Films made of PEG- and amide-functionalized CNTs exhibit lower conductivity, with the percolation transition taking place at higher average film thicknesses of ∼0.2 and ∼0.3 nm, respectively, compared to those of the PABS and carboxyl-functionalized samples having such threshold values below 0.1 nm (see Table 1).

The considerably different electrical conductivity values of the films at equivalent carbon nanotube coverage are a consequence of several factors related to film morphology and functional groups linked on the nanotubes. The homogeneity of networks on the substrate surface can play an important role since the formation of CNT bundles inherently results in a partial network of metallic ropes instead of individual metallic and semiconducting nanotubes. Bundling is caused by attractive forces of tube-to-tube van der Waals interac-
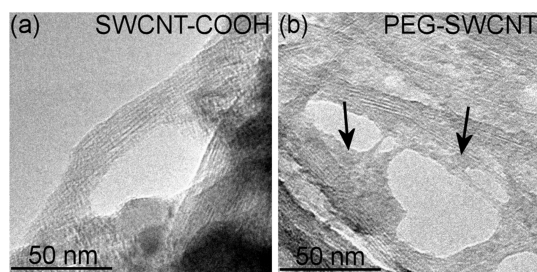
Figure 2. Transmission electron micrographs of (a) carboxylic acid and (b) poly(ethylene glycol)-functionalized inks dried on sample holder grids. The arrows in panel b show thin polymer layers between the nanotubes (and bundles).

TABLE 2. Electrical Characteristics of SWCNTs Films[a]

	carboxyl	amide	PEG	PABS
$t_{1\ layer}$[a] (nm)	∼0.11	∼0.37	∼0.23	∼0.12
R[b] (MΩ)	0.62 ± 0.15	0.95 ± 0.23	248.3 ± 72.6	43.8 ± 11.2
on−off ratio[c]	1.3 ± 0.1	1.9 ± 0.4	70 ± 5	4.4 ± 1.6
Φ_b[d] (meV)	140	106	256	176
m[e]	16.6	20.2	21.7	11.4

[a]Thickness of a single print. [b]Resistance measured at −1 V source−drain bias. [c]Transistor on/off ratio measured using −200 and +200 V gate at −1 V source−drain bias. [d]Apparent average height of Schottky barriers at the junctions of metallic and semiconducting nanotubes. [e]Average number of junctions along a percolated path in the network.

tions after the evaporation of solvent (water) from the ink. The forces can be especially strong for carboxyl and amide groups due to intermolecular H-bonding[25] between H and O or N along the side groups of adjacent nanotubes. For polymer side groups, the polymers can cause considerable steric hindrance and limitations in direct lapping of nanotubes on each others; that is, the nanotubes are somewhat separated from each other by the polymer chains (see Figure 2).

Another important factor is the acidic nature of the chemical group. Due to water adsorption on the nanotubes from the moisture of ambient air, carboxyl[26] and sulfonic acid[27] groups can deprotonate, thus providing mobile carriers (protons and hydronium ions) for electrical transport in the film. Accordingly, nanotube films with PEG functional groups that are insulating are expected to be the least conductive, while carboxyl-functionalized nanotubes are the most conductive due to possible bundling and protonic conduction. These assumptions are in qualitative agreement with the experimental results.
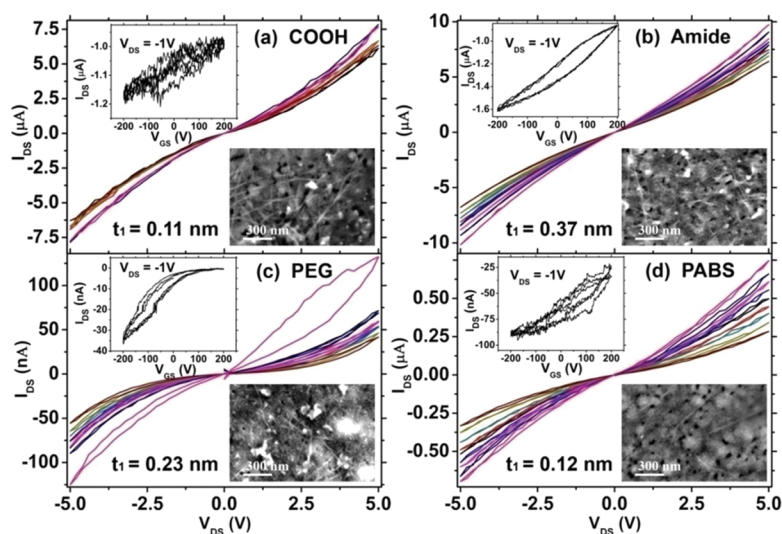
Films of carboxyl-functionalized SWCNTs exhibiting nonlinear $I-V$ characteristics are obtained if the entangled network has low nanotube density to allow formation of continuous electrical paths.[15−17] We find similar nonlinear electrical transport behavior for low density nanotube films functionalized with amide, PEG, and PABS functional groups, as shown in Figure 3.

The tunable channel transport by an external electric field (see insets in Figure 3) supports the existence of Schottky junctions in each nanotube network. Films of PEG- and PABS-SWCNTs have considerable gate effect with channel on/off ratios of ∼70 and ∼4.5, respectively, while the carboxyl- and amide-functionalized films show moderate gate response with channel on/off ratios of ∼1.3 and ∼2.0, respectively (Table 2). The higher channel conductance at negative gate voltages for each sample suggests similar p-type field-effect transistor operation regardless of the functional group linked to the nanotubes.

In order to quantify the height of the Schottky barriers (Φ_b) for the junctions of metallic and semiconducting nanotubes in each low density network, we apply a modified diode equation which takes into account the Ohmic losses and the series of several Schottky junctions in the percolated path. Thus the current in the nanotube networks is described as[16] $I(V,T) = AA^*T^2\exp(-\Phi_b/k_BT)[\exp(q(V - RI)/m)/(k_BT) - 1]$, where A is the average cross section of the films estimated by the film thickness and geometry, $A^* = 4\pi mqk^2/h^3$ is the Richardson constant, q is the elementary charge, $m^* = 0.037m_e$ is the effective mass of carriers in a nanotube,[28] k_B is Boltzmann's constant, h is Planck's constant, Φ_b is the Schottky barrier height, R is the serial resistance of the network obtained from the $I-V_{DS}$ slope at the large bias voltages, and m is the number of junctions along a percolated path (note, m is originally the ideality factor of the diode, which is considered to be 1 in our calculations). The nanotube−metal electrode interfaces are assumed to be Ohmic because of the large work function of Pt film ($\Phi_{Pt} > 5$ eV).[29,30] Fitting

Figure 3. Drain−source current−voltage $I_{DS}-V_{DS}$ sweeps for (a) COOH-, (b) CONH$_2$-, (c) PEG-, and (d) PABS-functionalized SWCNT films with thicknesses of 0.11, 0.37, 0.23, and 0.12 nm, respectively. The top insets are plots of $I_{DS}-V_G$ sweeps measured at −1 V channel bias (each averaged of three subsequent measurement cycles). The bottom insets are FESEM images of the corresponding nanotube networks. Note: transistor channel with COOH-functionalized nanotubes is printed using diluted ink (50% stock dispersion and 50% deionized water).
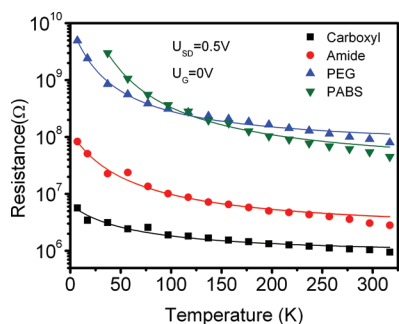
Figure 4. Channel resistance as a function of temperature measured using $U_{SD} = 0.5$ V. The lines are fit to thermally assisted tunneling with tunnel barriers of 12 ± 6, 22 ± 5, 19 ± 1, and 31 ± 2 meV for the carboxyl-, amide-, PABS-, and PEG-functionalized nanotube films, respectively.

the above equation on the measured $I-V_{DS}$ data, we get both Φ_b and m parameters (summarized in Table 2). The calculated average barrier heights from 106 to 256 meV are reasonable considering the barrier of a metal−semiconductor junction $\Phi_b = E_g - \Phi_m + \chi_s$, with a typical work function (Φ_m) of 4.5−5.0 eV for metallic CNTs as well as band gap (E_g) of 0.3−0.9 eV and electron affinity (χ_s) of 3.9−4.8 eV for semiconducting CNTs.[29−33] The electrodes (spacing gap of 15 μm) are connected with individual and bundled nanotubes having a length of ~1 μm, thus the number of Schottky junctions in series we estimate from the fitting parameters ($m = 11.4$ to 21.7) is also reasonable.

For PEG- and PABS-SWCNT films, the resistance is governed by the sum of the series resistance of the CNT itself, the junction resistance between the CNTs, and the resistance of the polymer layer between the CNTs. This explains the high resistance of the film, while the high nonlinear behavior could be explained by a high Schottky barrier (Φ_b). In this case, not only the metallic and semiconducting CNTs form junctions (*i.e.*, m-CNT/m-CNT, m-CNT/s-CNT, and s-CNT/m-CNT) but also m-CNT/polymer/m-CNT, m-CNT/polymer/s-CNT, and s-CNT/polymer/s-CNT interfaces can contribute to the nonlinear characteristics of such films.

The negative temperature coefficient of resistance measured for each sample from 7 to 317 K (Figure 4) shows nonmetallic electrical behavior similar to those results obtained by other groups.[17,23] However, a network of Schottky junctions seems to explain well the carrier transport near room temperature.[16,17] By fitting the diode equation to the low temperature data, we obtain an unreasonable match. Variable-range hopping proposed for thin single-wall carbon films[17] does not explain the process either; however, thermally assisted tunneling,[23] $R(T) = C\exp(T_b/(T_s + T))$, where $R(T)$ is the temperature-dependent resistance, C is a geometry parameter, T_b is the tunneling barrier height, and T_s/T_b is the quantum-induced tunneling in the absence of fluctuations, gives nearly perfect fit especially for data below ~200 K for each type of nanotube film just like in the case of pristine and carboxyl-functionalized nano-

tube films of various thicknesses measured by another group.

At low temperatures, the s-CNTs become insulating, thus electron tunneling between adjacent metallic nanotubes takes over the charge transport. The calculated apparent barrier energies are between 12 and 31 meV, slightly higher than those measured for CNT bundles, ~6,[34] ~9,[35] and ~7 meV for spray-coated films.[23]

On the basis of the results obtained for our inkjet-printed thin film transistors on Si chips, we inkjet-deposited entirely CNT-based FETs on a flexible polymer substrate (Figure 5a,b). Because of the measured highest on−off ratio for the channel current, PEG-functionalized nanotubes are selected to print the thin p-type channels (thickness of ~1.5 nm) on the surface of an ordinary transparency foil (Canon B-400). First, well-conducting electrodes using carboxylated nanotubes (~3.5 nm) are deposited for source and drain electrodes. These electrodes are then connected by the channel layer of PEG-functionalized CNTs. A layer of PEG (~20 μm) is then deposited on the top of the channel (and partly on the source and drain electrodes, too) to form the gate dielectric. Finally, on the top of the PEG film, the gate electrode (~3.5 nm) is printed using carboxylated nanotubes again. The as-made devices show nonlinear channel $I-V$ behavior and p-type FET operation with a typical on−off ratio ~3 with gate voltages between −3 and 3 V, as seen in Figure 5c. When the upper and lower limits of the gate bias sweeps are increased, the transistors show ambipolar characteristics (Figure 5d−f); however, when applying low gate voltages again, most of the devices operate as an n-channel FET, as shown in Figure 5g. Similar n-doping was observed for individual p-type nanotubes by using vacuum annealing[36] or by applying large gate bias while sourcing the channel of a p-FET device.[37] Both processes result in desorption of O_2 and other oxidizing moieties from the surface of nanotubes that are suggested to be responsible for p-type doping in ambient conditions.[37] Carrier mobilities (μ) up to ~60 cm^2 V^{-1} s^{-1} were obtained as calculated from the transfer curves and from the geometry of transistors according to $\mu = (L/WC_0)(1/V_{DS})\partial I_{DS}/\partial V_{GS}$, where $L = 250$ μm is the channel length, $W = 200$ μm is the channel width, and $C_0 \sim 7.7 \times 10^{-6}$ A s V^{-1} m^{-2} is the gate capacitance. These values are about an order of magnitude lower than those measured for aligned single-wall nanotube array devices.[38]

CONCLUSIONS

We have studied the electrical properties of inkjet-deposited thin films of four different types of functionalized single-wall carbon nanotubes and confirmed the important role of chemical functionalization on the electrical properties SWCNT networks. We found that the films behave as percolating networks with a power law depen-
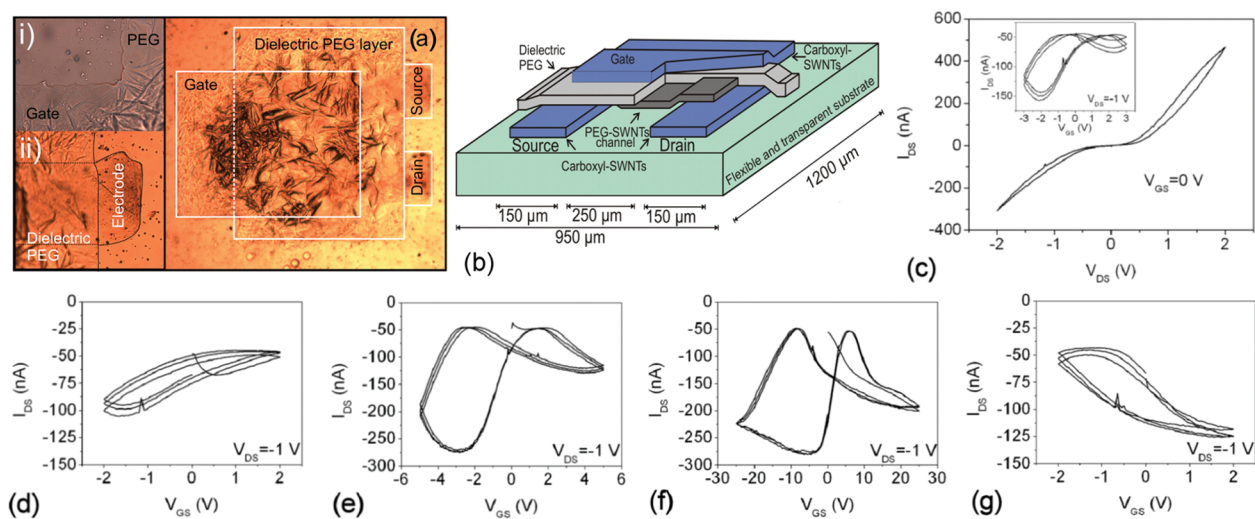
Figure 5. Entirely inkjet-printed FET with PEG-functionalized SWCNT thin film as channel, COOH-functionalized SWCNT film electrodes (source, drain, and gate), and PEG film as gate dielectric on a flexible transparency foil. (a) Optical micrograph and (b) schematic drawing of the device. (c) $I_{DS}-V_{DS}$ at $V_{GS} = 0$ V and $I_{DS}-V_{GS}$ at $V_{DS} = -1$ V plots of a transistor showing p-channel behavior. (d−g) $I_{DS}-V_{GS}$ plots of a device measured using different gate bias sweeps. The applied external electrical field results in gradual n-doping of the p-type channel: (d) p-FET at -2 V $< V_{GS} < 2$ V, (e) p-FET with slightly ambipolar behavior at -5 V $< V_{GS} < 5$ V, (f) ambipolar operation at -25 V $< V_{GS} < 25$ V, and (g) n-type FET device operation after lowering the gate voltage sweep again to -2 V $< V_{GS} < 2$ V.

dence of the conductivity on the film thickness, showing quasi-one-dimensional charge transport. The electrical transport near room temperature could be well explained by thermionic emission, taking place at the junctions between crossing semiconducting and metallic nanotubes. Polymeric functionalization shows decreased conductivity by 1−2 orders of magnitude when compared to the amide- and carboxyl-functionalized nanotube films of the corresponding thickness and exhibits higher apparent average Schottky barriers.

When using a proper selection of functional groups and film thickness, it is possible to obtain film conductivities in a large parameter window. By simply changing the layer thickness, networks with linear as well as nonlinear gate-controllable current−voltage transport can be made with all types of nanotubes. Though the on−off ratios obtained for functionalized SWCNT thin film transistors are moderate compared to those measured on individual nanotubes, such components can be still practical (e.g., for low-end devices that are produced in large quantities) since any preselection of individual semiconducting nanotubes is not necessary. Furthermore, with a proper optimization of gate dielectric material and thickness, the switching behavior might be improved further.

At low temperatures, the semiconducting nanotubes become insulating, thus electron tunneling between adjacent metallic nanotubes takes over the charge transport.

Finally, we have successfully demonstrated that inkjet-printed field-effect transistors could be constructed solely from thin films of functionalized car-

TABLE 3. General Characteristics of Water-Based SWCNT Inks

SWCNTs type	Fraction of functional group[a] (wt%)	Measured solid content[b] (µg/mL)	CNT content[c] (µg/mL)	Structure
Carboxyl (-COOH)	14.9	28 ± 3	~24	
Amide (-CONH₂)	13.2	46 ± 5	~40	
poly(ethylene glycol) (PEG)	30	35 ± 4	~25	
poly(aminobenzene sulfonic) acid (PABS)	65	38 ± 4	~13	

[a]The wt % values of functional groups are according to the specifications of Sigma-Aldrich. [b]The values correspond to the whole amount of solid content in the inks measured by filtration of 10 mL ink from each sample. [c]The values show the nanotube concentration obtained from (a) and (b).

bon nanotubes (except the gate dielectric, which is a layer of inkjet-printed PEG). We have also shown that a p-channel thin film FET device could be transformed to n-type by simply applying a large local electrical field with the gate electrode. Because of practical reasons (to enable easy contacting with probes for electrical testing), the current size of a printed transistor is $\sim 1 \times 1$ mm^2, which could be scaled down to a size of $\sim 100 \times 100$ μm^2 with $\sim 35-35$ μm channel length and width considering the diameter of ~ 35 μm for the dried ink droplets having a nominal volume of ~ 10 pL ejected from the cartridge. Any further decrease of transistor size is possible only by using inkjet heads producing smaller ink drops or by applying substrates that are pretreated to have hydrophilic and hydrophobic surface areas for enabling good ink localization on the surface.[39]

EXPERIMENTAL SECTION

Four types of SWCNTs with different chemical functionalization, such as carboxylic acid ($-$COOH), amide ($-$CONH$_2$), poly-(ethylene glycol) (PEG), and polyaminobenzene sulfonic acid (PABS), were used as purchased from Sigma-Aldrich. Inkjet-printable aqueous dispersions of SWCNTs were prepared by sonicating 2.0 mg of nanotubes in 15 mL of deionized water for 3$-$5 h. Subsequently, the dispersions were centrifuged at 3500 rpm for 30 min, and the supernatant solution was collected and centrifuged again for 15 min. The centrifugation and separation steps were repeated at least four times. The as-obtained inks (Table 3) were then inkjet-printed on customized Si chips using a DIMATIX Fujifilm DMP-2831 with 10 pL nominal drop volume.

Boron-doped p$^+$ Si substrate (5$-$20 m$\Omega \cdot$cm) with a thin evaporated layer of Al on its bottom was used as back-side gate electrode. SiO$_2$ layer of ~ 1 μm (PECVD) was applied as gate dielectric on which electrodes of Pt on Ti (thickness of 300 nm and 45 nm, respectively) were defined by optical lithography. The spacing gap between adjacent source$-$drain electrodes was 15 μm.

In order to deposit thin films with different average nanotube thickness, multiple prints over the same pattern were made. The test patterns were lines with a length of ~ 200 μm deposited with 9 ink droplets of 25 μm center-to-center spacing. The diameter of the dried droplets was typically ~ 35 μm for each ink. The average layer thickness values for the nanotube films were calculated as $t = c_{ink} \times V_{drop} \times N_{drop} \times (\rho_{SWCNT} \times A_{pattern})^{-1}$, where c_{ink} is the ink concentration measured by weighing the mass of solid residuals after filtrating each ink (and normalizing it to the carbon content by considering the weight fraction of functional groups), V_{drop} is the nominal drop volume of 10 pL, N_{drop} is the number of drops over the printed area ($A_{pattern}$), and $\rho_{SWCNT} = 1.4$ g$\cdot$cm^{-3} is the mass density of a SWCNT.

The electrical characterization of each sample was carried out in ambient conditions using a dual source meter (Keithley 2612) with LabView control.

Low-temperature measurements were performed in vacuum (base pressure $\sim 4 \times 10^{-6}$ mbar). The sample was connected in series with a resistor ($R \ll R_{Sample}$) and a SIM928 isolated voltage source (Stanford Research Systems). As voltage was applied across the sample, the corresponding current was measured over the resistor R. The signal was amplified and detected with a SIM BJT preamplifier (Stanford Research Systems) and an Agilent 34401A digital multimeter, respectively. Optistat AC-V PT cooler system (OXFORD INSTRUMENTS) has been used in temperature control. The sample was attached to the cold head, and a vacuum was pumped with TURBO-V 70 LP MacroTorr (VARIAN) into the measurement chamber. Cooling was performed with a Pulse Tube refrigerator, whereas the heating was adjusted with an Intelligent Temperature Controller (ITC503) to reach the desired temperature. Data acquisition was performed automatically using LabVIEW 8.2.

REFERENCES AND NOTES

1. Avouris, P. Molecular Electronics with Carbon Nanotubes. *Acc. Chem. Res.* **2002**, *35*, 1026–1034.
2. Bachtold, A.; Hadley, P.; Nakanishi, T.; Dekker, C. Logic Circuits with Carbon Nanotube Transistors. *Science* **2001**, *294*, 1317–1320.
3. Kong, J.; Franklin, N. R.; Zhou, C. W.; Chapline, M. G.; Peng, S.; Cho, K. J.; Dai, H. J. Nanotube Molecular Wires as Chemical Sensors. *Science* **2000**, *287*, 622–625.
4. Collins, P. G.; Zettl, A.; Bando, H.; Thess, A.; Smalley, R. E. Nanotube Nanodevice. *Science* **1997**, *278*, 100–103.
5. Zhou, Y. X.; Gaur, A.; Hur, S. H.; Kocabas, C.; Meitl, M. A.; Shim, M.; Rogers, J. A. p-Channel, n-Channel Thin Film Transistors and p$-$n Diodes Based on Single Wall Carbon Nanotube Networks. *Nano Lett.* **2004**, *4*, 2031–2035.
6. Meitl, M. A.; Zhou, Y. X.; Gaur, A.; Jeon, S.; Usrey, M. L.; Strano, M. S.; Rogers, J. A. Solution Casting and Transfer Printing Single-Walled Carbon Nanotube Films. *Nano Lett.* **2004**, *4*, 1643–1647.
7. Bradley, K.; Gabriel, J.-C. P.; Grüner, G. Flexible Nanotube Electronics. *Nano Lett.* **2003**, *3*, 1353–1355.
8. Snow, E. S.; Novak, J. P.; Campbell, P. M.; Park, D. Random Networks of Carbon Nanotubes as an Electronic Material. *Appl. Phys. Lett.* **2003**, *82*, 2145–2147.
9. Mäklin, J.; Mustonen, T.; Kordas, K.; Saukko, S.; Toth, G.; Vähäkangas, J. Nitric Oxide Gas Sensors with Functionalized Carbon Nanotubes. *Phys. Status Solidi B* **2007**, *244*, 4298–4302.
10. Varghese, O. K.; Kichambre, P. D.; Gong, D.; Ong, K. G.; Dickey, E. C.; Grimes, C. A. Gas Sensing Characteristics of Multi-Wall Carbon Nanotubes. *Sens. Actuators, B* **2001**, *81*, 32–41.
11. Wu, Z. C.; Chen, Z. H.; Du, X.; Logan, J. M.; Sippel, J.; Nikolou, M.; Kamaras, K.; Reynolds, J. R.; Tanner, D. B.; Hebard, A. F.; Rinzler, A. G. Transparent, Conductive Carbon Nanotube Films. *Science* **2004**, *305*, 1273–1276.
12. Barnes, T. M.; Wu, X.; Zhou, J.; Duda, A.; van de Lagemaat, J.; Coutts, T. J.; Weeks, C. L.; Britz, D. A.; Glatkowski, P. Single-Wall Carbon Nanotube Networks as a Transparent Back Contact in CdTe Solar Cells. *Appl. Phys. Lett.* **2007**, *90*, 243503.
13. de Andrade, M. J.; Lima, M. D.; Skakalova, V.; Bergmann, C. P.; Roth, S. Electrical Properties of Transparent Carbon Nanotube Networks Prepared through Different Techniques. *Phys. Status Solidi RRL* **2007**, *1*, 178–180.
14. Kordás, K.; Mustonen, T.; Toth, G.; Jantunen, H.; Lajunen, M.; Soldano, C.; Talapatra, S.; Kar, S.; Vajtai, R.; Ajayan, P. M. Inkjet Printing of Electrically Conductive Patterns of Carbon Nanotubes. *Small* **2006**, *2*, 1021–1025.
15. Beecher, P.; Servati, P.; Rozhin, A.; Colli, A.; Scardaci, V.; Pisana, S.; Hasan, T.; Flewitt, A. J.; Robertson, J.; Hsieh, G. W.; Li, F. M.; Nathan, A.; Ferrari, A. C.; Milne, W. I. Ink-Jet Printing of Carbon Nanotube Thin Film Transistors. *J. Appl. Phys.* **2007**, *102*, 043710.

16. Mustonen, T.; Maklin, J.; Kordas, K.; Halonen, N.; Toth, G.; Saukko, S.; Vähäkangas, J.; Jantunen, H.; Kar, S.; Ajayan, P. M.; Vajtai, R.; Helisto, P.; Seppa, H.; Moilanen, H. Controlled Ohmic and Nonlinear Electrical Transport in Inkjet-Printed Single-Wall Carbon Nanotube Films. *Phys. Rev. B* **2008**, *77*, 125430.

17. Skákalová, V.; Kaiser, A. B.; Woo, Y. S.; Roth, S. Electronic Transport in Carbon Nanotubes: From Individual Nanotubes to Thin and Thick Networks. *Phys. Rev. B* **2006**, *74*, 085403.

18. Geng, H. Z.; Kim, K. K.; So, K. P.; Lee, Y. S.; Chang, Y.; Lee, Y. H. Effect of Acid Treatment on Carbon Nanotube-Based Flexible Transparent Conducting Films. *J. Am. Chem. Soc.* **2007**, *129*, 7758–7759.

19. Zhao, J. J.; Park, H. K.; Han, J.; Lu, J. P. Electronic Properties of Carbon Nanotubes with Covalent Sidewall Functionalization. *J. Phys. Chem. B* **2004**, *108*, 4227–4230.

20. Park, H.; Zhao, J. J.; Lu, J. P. Effects of Sidewall Functionalization on Conducting Properties of Single Wall Carbon Nanotubes. *Nano Lett.* **2006**, *6*, 916–919.

21. Kim, S.; Lee, H. R.; Yun, Y. J.; Ji, S.; Yoo, K.; Yun, W. S.; Koo, J. Y.; Ha, D. H. Effects of Polymer Coating on the Adsorption of Gas Molecules on Carbon Nanotube Networks. *Appl. Phys. Lett.* **2007**, *91*, 093126.

22. Zhang, T.; Mubeen, S.; Bekyarova, E.; Yoo, B. Y.; Haddon, R. C.; Myung, N. V.; Deshusses, M. A. Poly(*m*-aminobenzene sulfonic acid) Functionalized Single-Walled Carbon Nanotubes Based Gas Sensor. *Nanotechnology* **2007**, *18*, 165504.

23. Bekyarova, E.; Itkis, M. E.; Cabrera, N.; Zhao, B.; Yu, A. P.; Gao, J. B.; Haddon, R. C. Electronic Properties of Single-Walled Carbon Nanotube Networks. *J. Am. Chem. Soc.* **2005**, *127*, 5990–5995.

24. Stauffer, D. Aharony, A. *Introduction to Percolation Theory*; Taylor & Francis: London, 1994.

25. Shriver, D. F.; Atkins, P. W. *Inorganic Chemistry*; Oxford University Press: New York, 2006.

26. Hu, H.; Ni, Y. C.; Montana, V.; Haddon, R. C.; Parpura, V. Chemically Functionalized Carbon Nanotubes as Substrates for Neuronal Growth. *Nano Lett.* **2004**, *4*, 507–511.

27. Paddison, S. J. Proton Conduction Mechanisms at Low Degrees of Hydration in Sulfonic Acid-Based Polymer Electrolyte Membranes. *Annu. Rev. Mater. Res.* **2003**, *33*, 289–319.

28. Jarillo-Herrero, P.; Sapmaz, S.; Dekker, C.; Kouwenhoven, L. P.; van der Zant, H. S. J. Electron-Hole Symmetry in a Semiconducting Carbon Nanotube Quantum Dot. *Nature* **2004**, *429*, 389–392.

29. Manohara, H. M.; Wong, E. W.; Schlecht, E.; Hunt, B. D.; Siegel, P. H. Carbon Nanotube Schottky Diodes Using Ti-Schottky and Pt-Ohmic Contacts for High Frequency Applications. *Nano Lett.* **2005**, *5*, 1469–1474.

30. Su, W. S.; Leung, T. C.; Chan, C. T. Work Function of Single-Walled and Multiwalled Carbon Nanotubes: First-Principles Study. *Phys. Rev. B* **2007**, *76*, 235413.

31. Appenzeller, J.; Radosavljevic, M.; Knoch, J.; Avouris, P. Tunneling *versus* Thermionic Emission in One-Dimensional Semiconductors. *Phys. Rev. Lett.* **2004**, *92*, 048301.

32. Buonocore, F.; Trani, F.; Ninno, D.; Di Matteo, A.; Cantele, G.; Iadonisi, G. *Ab Initio* Calculations of Electron Affinity and Ionization Potential of Carbon Nanotubes. *Nanotechnology* **2008**, *19*, 025711.

33. Kazaoui, S.; Minami, N.; Matsuda, N.; Kataura, H.; Achiba, Y. Electrochemical Tuning of Electronic States in Single-Wall Carbon Nanotubes Studied by *In Situ* Absorption Spectroscopy and AC Resistance. *Appl. Phys. Lett.* **2001**, *78*, 3433–3435.

34. Kaiser, A. B.; Düsberg, G.; Roth, S. Heterogeneous Model for Conduction in Carbon Nanotubes. *Phys. Rev. B* **1998**, *57*, 1418–1421.

35. Kaiser, A. B.; McIntosh, G. C; Edgar, K.; Spencer, J. L.; Yu, H. Y; Park, Y. W. Some Problems in Understanding the Electronic Transport Properties of Carbon Nanotube Ropes. *Curr. Appl. Phys.* **2001**, *1*, 50–55.

36. Avouris, P. Carbon Nanotube Electronics. *Chem. Phys.* **2002**, *281*, 429–445.

37. Javey, A.; Wang, Q.; Ural, A.; Li, Y.; Dai, H. Carbon Nanotube Transistor Arrays for Multistage Complementary Logic and Ring Oscillators. *Nano Lett.* **2002**, *2*, 929–932.

38. Kang, S. J; Kocabas, C.; Ozel, T.; Shim, M.; Pimparkar, N.; Alam, M. A.; Rotkin, S. V.; Rogers, J. A. High-Performance Electronics using Dense, Perfectly Aligned Arrays of Single-Walled Carbon Nanotubes. *Nat. Nanotechnol.* **2007**, *2*, 230–236.

39. Sirringhaus, H.; Kawase, T.; Friend, R. H.; Shimoda, T.; Inbasekaran, M.; Wu, W.; Woo, E. P. High-Resolution Inkjet Printing of All-Polymer Transistor Circuits. *Science* **2000**, *290*, 2123–2126.